Insights on thickness-dependent charge transfer efficiency modulated by ultrasonic treatment in hematite photoanodes

Andre L. M. Freitas^{1,2,*}, Aryane Tofanello², Flavio L. Souza^{2,3,**} and Yat Li^{1,&}

¹Department of Chemistry and Biochemistry, University of California, Santa Cruz, California, 95064 USA.

²Laboratory of Alternative Energy and Nanomaterials (LEAN), Universidade Federal do ABC (UFABC), 09210-580, Santo André, SP, Brazil.

³Brazilian Nanotechnology National Laboratory (LNNano), 13083-100, Campinas, SP, Brazil.

Corresponding authors

 $* and re_luizmf@yahoo.com.br; **flavio.souza@ufabc.edu.br; \&yatli@ucsc.edu$

Abstract

The comprehension of the solid-liquid interface associated with the poor charge carrier dynamic of hematite has prevented its commercial application as a photoanode in a photoelectrochemical cell. The development of a low-cost and scalable strategy to overcome such drawbacks is yet pursued by the scientific community. Here, a simple surface modification of hematite photoanode designed with different thickness was performed employing ultrasonic treatment (UST) process. UST creates an inhomogeneous defect distribution based on the solid-liquid energetics. The thicker photoanodes (H-4h) showed that the mechanical process can contribute to remove unstable layers,

creating favorable sites for oxygen evolution without compromise the solid-solid interface. UST approach for H-2h has promoted surface states pinning and possibly increased the stress in between hematite-FTO. The effects on thinner photoanodes (H-2h) can drastically create polarized states that enhance surface trapping states, reducing the photogenerated charge lifetime. The outcome findings reveal that the surface hydroxylation might be extremely dependent on the electrode thickness. This study indicates that the UST approach is an efficient tool to boost thicker photoanodes performance, as desired for practical applications. Thus, for thinner layers, the stress induced at the hematite-FTO interface can be aggravated by mechanical treatment overcoming the beneficial effects at the solid-liquid interface. In fact, hydroxylation conducted via the sonication process is highly recommended for designing thicker films.

1. Introduction

Hematite, owing to its excellent chemical stability and favorable band gap, has been widely investigated as a photoanode for photoelectrochemical (PEC) hydrogen generation. ^{1–5} However, its performance is limited by several factors, including weak light absorption, inefficient charge separation and slow surface kinetics. A major effort in the community is to understand the surface reactions and transport properties of hematite photoanodes. ^{6–10} Numerous methods have been employed to improve the oxygen evolution reaction (OER) efficiency such as oxygen vacancies incorporation, ^{11–13} doping engineering (*in-situ* and *ex-situ*), ^{14–18} and high temperature treatments. ^{19–21} Many of these methods enhance the PEC performance of hematite via surface modification. Previous reports have demonstrated that the intentional doping of Sn or Sb can significantly increase the carrier density of hematite, favoring an efficient charge separation and, thus, its photocatalytic performance. ^{15,22–25} Some of these surface modifications successfully

promote OER by accelerating the photogenerated charge transfer and reducing the charge resistance at the solid-liquid interface. 16,26,27

The kinetics at the interface are closely related to the surface states, which can facilitate or trap photogenerated charges. Despite previous efforts to boost the hematite performance, all reports show that there is room for improvement, and the carrier dynamics on the hematite surface is an interesting area for further exploration. In recent years, a considerable number of strategies for incorporating OH species onto hematite surfaces have been discussed. An attractive way to activate oxide surfaces with these functional groups is the use of mechanical processes mediated by ultrasound technique. The main reactions, including the free radical formation by sonication, can be described as follows: 28,29

$$H_2O \xrightarrow{))))} H + OH$$
 (Reaction 1)

$$OH + OH \xrightarrow{))))} H_2O_2$$
 (Reaction 2)

$$H_2O_2 + OH^{\cdot} \xrightarrow{))))} HOO^{\cdot} + H_2O$$
 (Reaction 3)

In water, the complete reaction involved in the ultrasonic process leads to the formation of several free radicals as mentioned in the reactions 1, 2 and 3; including peroxide as well described in the literature.³¹ However, dealing with the sonication power and exposure time, it is possible to limit the reaction only to the hydroxyl formation (reaction 1) at short time, avoiding access to other radicals that may be interesting to other applications. In the photocatalytic process, the overall efficiency is governed by several factors, including a change in the ionization state of the semiconductor surface, which affects not only the adsorption mode, but also the selectivity towards reactants, since the redox reactions in the photochemical process are sensitive surface potential variations. Additionally, the presence of different species or complexes on the semiconductor surface can alter the electron-hole dynamics and, thus, the efficiency of photocatalysis. In the

ultrasound process, the hematite surface states are strongly influenced by its interaction with water molecules, which are highly dependent on the coordination number of Fe atoms and the surface composition.³² In this condition, there are mainly two hydroxyl moieties on the hematite surface: terminal hydroxyl groups (Fe-OH) and bridging hydroxyl groups (O_x-H). Because of the chemistry of surface defects associated with the effect of ultrasonic treatment, OH⁻ ions are expected to migrate between the interconnected defective crystallite boundaries, while H₃O⁺ ions diffuse through proton hopping at the surface.³³

Carvalho and co-workers³⁴ investigated that the oxygen evolution reactions are governed by an initial slow step of oxy-hydroxide group formation on the electrode surface, which possibly limits the PEC performance. Nonetheless, the use of methods that promote surface hydroxylation has been investigated and points out certain controversies among different groups. Li *et al.*³⁵ demonstrated a strategy and the importance of removing surface states, classified as trap states, acquired by the presence of hydroxyl species in the solid-liquid interface that limits the photogenerated charge mobility. On the other hand, Fábrega and co-workers³⁶ investigated the water photo-oxidation conducted by TiO₂ and revealed that the trapping states on the surface play an important role as intermediates in surface reactions. The hydroxyl states on the surface contributed to an increase in the photogenerated charge lifetime reducing the electron-hole recombination.

In addition, Tang *et al.*³⁰ have recently demonstrated a simple and effective methodology to modify metal oxide surfaces, showing that the incorporation of OH states enhances the photogenerated charge carrier dynamics at the solid-liquid interface without compromising bulk properties. Hydroxylation effectively improved the photoelectrocatalytic performance without any changes in basic properties such as optical, electronic, and/or structural properties. Their work

showed that hydroxylated hematite surface induced by ultrasonic process mediates the hole transfer at the solid-liquid interface promoting an efficient OER, in which or wherein the only assigned variation is due to the OH-states incorporation; regardless of the solvent, time or ultrasound power used during experimental procedure.

Based on the literature propositions, it is well known that for thicker materials, surface modifications do not have a drastic impact on the metal oxide-substrate interface, and often present major positive effects related to the solid-liquid interface. ^{27,37} However, for thinner layers, there is a greater interaction between the layer and the substrate, which can approach the material as composed only of the surface. ^{38,39} In this sense, the mechanical stress involved in the hydroxylation process can significantly affect all homo- and/or hetero-interfaces of different thicknesses, achieving opposite results. Hydroxylation might contribute or accumulate effects that negatively affect the photoanodes efficiency. Herein, we report a study to understand how the hydroxylation processes mediated by ultrasonic treatment change the charge dynamics at the hydroxylate surface of hematite-based photoanodes with different thicknesses. We seek to distinguish and elucidate the charge transfer mechanism at the semiconductor-electrolyte interface and how the surface hydroxylation process can have different impacts.

2. Materials and Methods

Hematite nanowire arrays were prepared by a hydrothermal method reported previously. 1,23,26 A precursor solution containing 0.15 M of iron chloride (FeCl₃.6H₂O) and 1 M of sodium nitrate (NaNO₃) were prepared. A clean conductive glass substrate, FTO (F:SnO₂ / fluorine-doped tin oxide) was used as the growth substrate. The substrate and 30 mL of the precursor solution were transferred to a Teflon-lined stainless-steel autoclave. Two iron

oxyhydroxide (β -FeOOH) samples were obtained under hydrothermal conditions at 95 °C for 2 h and 4 h, respectively. After these processes, the obtained yellowish film was washed several times in water in order to remove all impurities resulting from the hydrothermal synthesis including chlorine ions adsorbed on the surface. The as-synthesized photoanodes were further annealed in air at 750°C for 30 min to convert the β -FeOOH phase into hematite (α -Fe₂O₃). The hematite sample was then placed (faced up) in a beaker filled with distilled water and subjected to a fast treatment in an ultrasonic bath (70W) for 10 s. After treatment, the sample was air-dried at room temperature.

The morphology of the hematite photoanodes was analyzed by FE-SEM using a dual-beam microscope (FEI Quanta 3D field emission microscope). The structural characterization was carried out by X-ray photoelectron spectroscopy (XPS) using a spectrometer (ScientaOmicron ESCA+) with a high-performance hemispheric analyzer (EAC2000) and an excitation source of monochromatic Al K α (hv = 1486.6 eV) radiation. The analysis was performed in an ultra-high vacuum chamber (UHV) at 10^{-9} Pa. XPS spectra were obtained at a constant pass energy of 20 eV with a step size of 0.05 eV.

The photoelectrochemical measurements were performed in a three-electrode configuration using a CHI 660D electrochemical workstation coupled with a solar simulator (Newport 6255) with a 1.5 AM Global filter, power adjusted at 100 mW cm⁻². Hematite photoanode was used as the working electrode. Ag/AgCl (sat. KCl) electrode and a Pt coil were used as the reference and counter electrodes, respectively. Linear sweep voltammograms were collected from -0.8 to 0.8 V vs. Ag/AgCl, in 1M KOH solution (pH=13.5) at a scan rate of 50 mV s⁻¹. Photoelectrochemical impedance spectroscopy (PEIS) was performed

in a frequency range from 1 mHz to 100 kHz using a potentiostat (CHI 660D) with an FRA analyzer and the results were analyzed using Z-view software with minimal fitting error dispersion.

The photogenerated charge carrier dynamics were investigated by transient absorption spectroscopy (TAS) using a spectrophotometer (Optical Building Blocks Corporation, OBB) and the measured signal was evaluated by a digital oscilloscope (Tek-tronic, TDS 2022C). The TAS configuration was composed of a nitrogen laser excitation pump (337 nm) and a monochromatic probe operating at a wavelength of 650 nm. The measurements were carried out under no bias and a 1.23 applied potential in alkaline (pH=13.5) electrolyte.

3. Results and discussion

Hematite-based photoanodes designed with different thicknesses under hydrothermal conditions were sonicated in distilled water for 10s and denoted as H-2h and H-4h (before) and SH-2h and SH-4h (after), respectively.

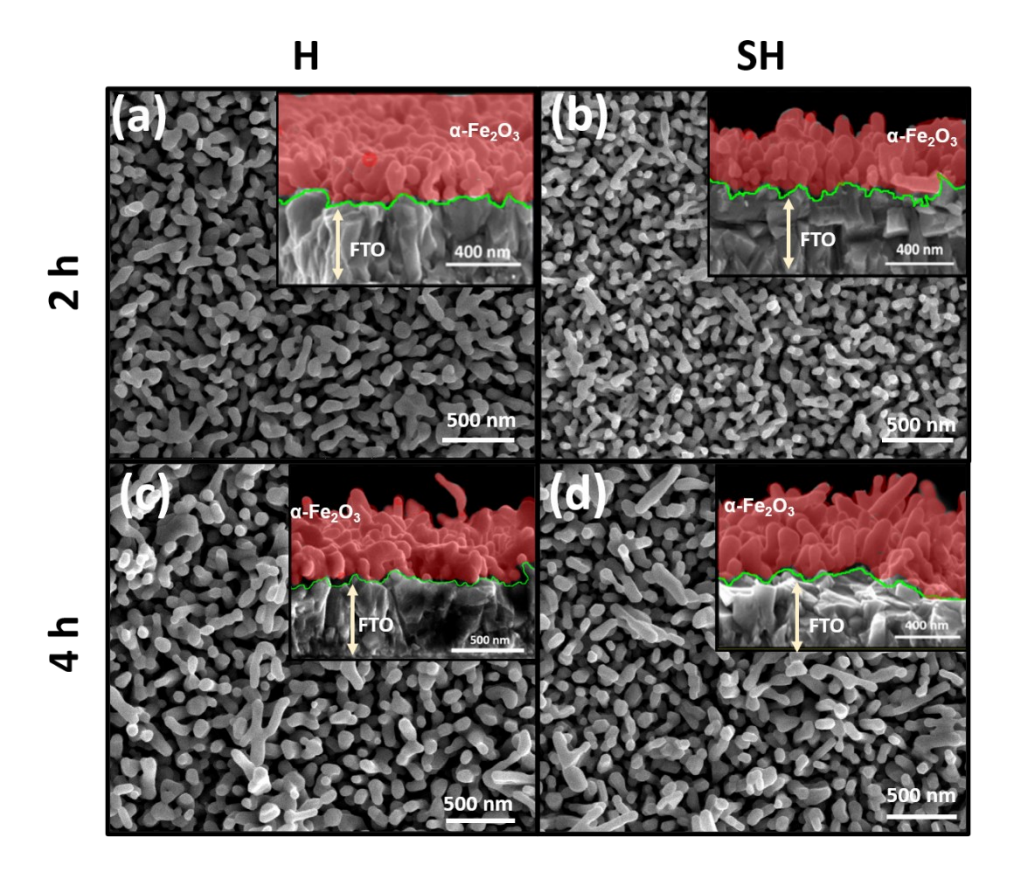


Figure 1. Top view FE-SEM images of (a) H-2h, (b) SH-2h, (c) H-4h and (d) SH-4h. Insets: Cross-sectional view FE-SEM images of the photoanodes.

The top and cross-sectional view FE-SEM images shown in **Figure 1** reveal the formation of a nanowire array morphology as expected, and using image software (*Image J*), the average nanowire lengths were calculated to be 166 ± 12 nm and 261 ± 11 nm for H/SH-2h and H/SH-4h, respectively. Moreover, no obvious morphological (nanowire length) change upon ultrasonication is observed corroborating with its non-destructive effect, as previously reported.³⁰ Interestingly, in the same report, it was noted that the ultrasonic treatment (UST) retained a similar electrochemical active area and did not lead to the formation of an amorphous layer on top of the hematite surface. The presence of micropores due to the UST process can be neglected.³⁰ To evaluate the surface hydroxilation due to the UST process and its possible dependence with hematite thickness,

photoelectrochemical measurements combined with several other techniques were employed.

Figure 2 shows the PEC performance of the hematite photoanodes before and after hydroxylation in the dark and under illumination.

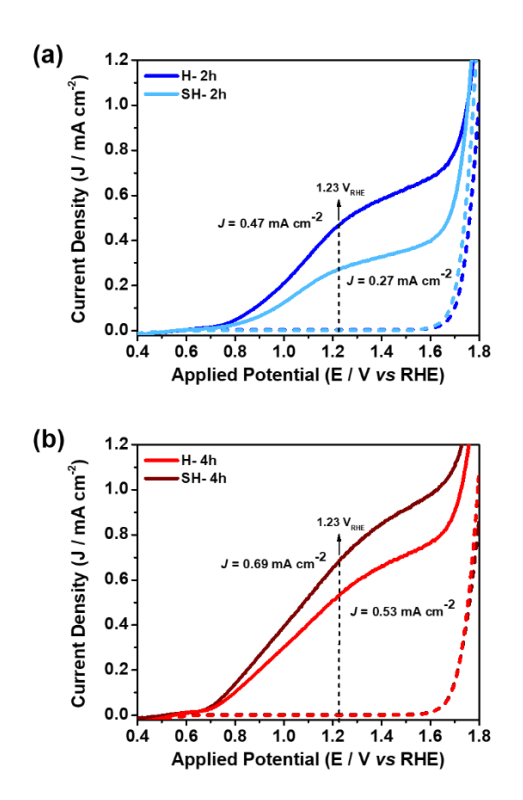


Figure 2. Linear sweep voltammetry (LSV) of hematite photoanodes (H-2h, SH-2h, H-4h and SH-4h) in 1M KOH electrolyte (pH=13.5) collected in the dark and under light illumination (Solar simulator + AM 1.5 G filter).

Despite the observed difference in hematite photoanode thickness, H-2h and H-4h exhibit a similar photocurrent, with a slight increase for H-4h. Interestingly, after ultrasonic treatment, the two photoanodes exhibited different photocurrent responses. The photocurrent density of H-2h decreased from 0.47 to 0.27 mA cm⁻² after sonication (**Figure 2a**). On the contrary, H-4h achieved an enhanced photocurrent from 0.53 to 0.69 mA cm⁻² (**Figure 2b**). Moreover, a triplicate study reinforces the opposite results acquired after the surface hydroxylation process in photoanodes with different thicknesses (**Figure S1**, **Supporting Information**). In this scenario, the better

phoelectrochemical response was observed for the thicker photoanode. Therefore, electrochemical impedance measurements (EIS) were performed to understand the electronic changes (**Figure 3**) and calculated parameters are summarized in **Table 1**.

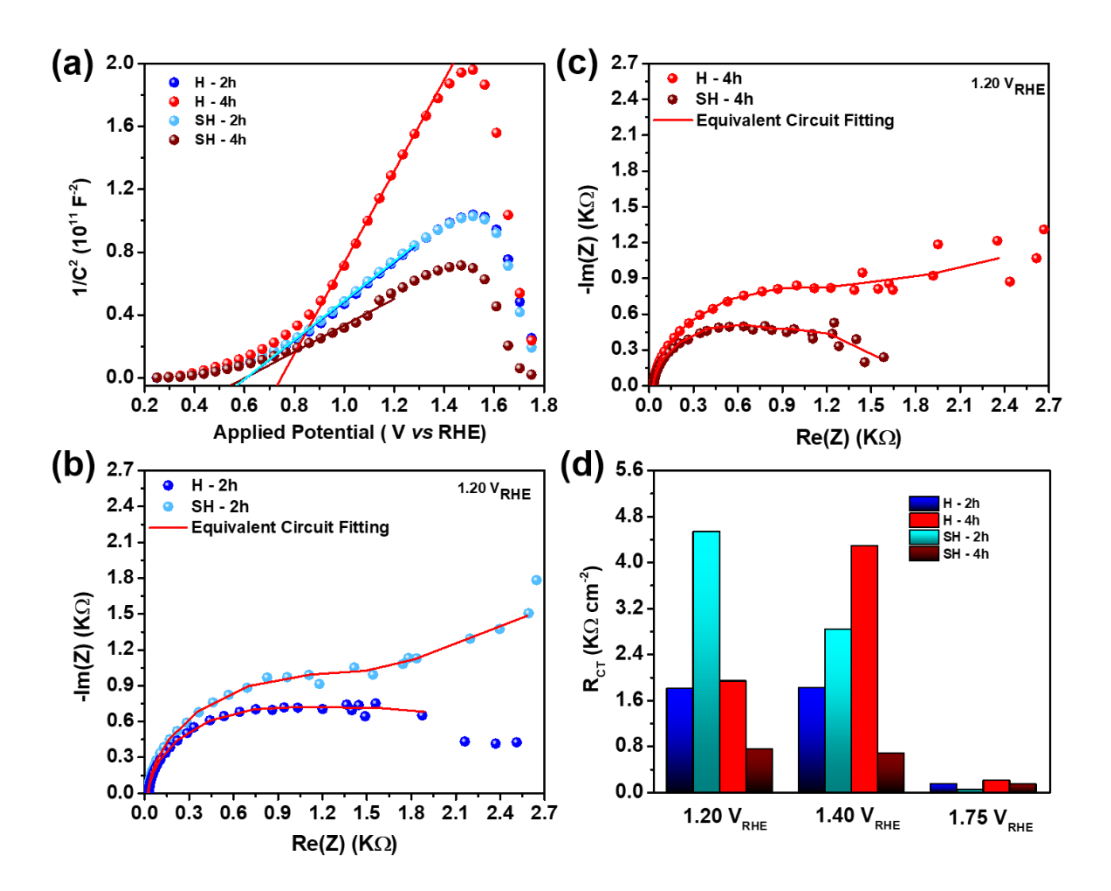


Figure 3. (a) Mott Schottky measurements performed with potential ranging 0.2-1.8 V_{RHE} ; Nyquist plots in aqueous electrolyte under solar simulated light conditions for: (b) H-2h and SH-2h, (c) H-4h and SH-4h; (d) Electrical parameters calculated from fitted equivalent circuit $R_s[R_{bulk}/C_{bulk}]$ [R_{CT}/C_{ss}]] where R_{CT} – resistance to charge transfer at solid-liquid interface for all photoanodes under three different applied potentials:1.2, 1.4 and 1.75 V_{RHE} .

Table 1. Electrochemical impedance parameters calculated from linear adjustment on Mott-Schottky analysis: Donors Density (N_d) , flat band potential (V_{fb}) and depletion layer length (W).

	J at 1.23 V _{RHE} (mA cm ⁻³)	N _d (10 ¹⁹ cm ⁻³)	V _{fb} (V _{RHE})	W (nm)
H-2h	0.47	5.70	0.58	16
H-4h	0.50	2.43	0.70	15
SH-2h	0.27	5.64	0.58	16
SH-4h	0.69	8.38	0.57	13

EIS and PEIS measurements were carried out at 1 mHz – 100 kHz. H-4h has a V_{fb} value higher than that of H-2h, in agreement with the visualized photocurrent response. The slight changes observed (**Table 1**) in the donor density number (N_D) within the same order of magnitude can be more associated with different film roughness (exposed area) and Mott-Schottky model limitation than the UST treatment. Therefore, normalizing the EIS data by the exposed geometric area (roughness) to the electrolyte during the measurements will probably show similar N_D values in between them. Based on this argument, the highest PEC performance exhibited by SH-4h is attributed to the UST surface activation. The pronounced change in the overall capacitance (**Figure 3a**) is a another strong indicative that the surface was the limiting factor to achieve PEC performance.

Based on this, PEIS was carried out to analyze the surface properties and Nyquist results (**Figure 3b-c**), revealing that UST has impacted differently for the hematite photoanodes; SH-2h has increased overall resistance while the resistance of SH-4h decreases after the UST process. Charge transfer resistance (R_{CT}) was calculated by applying equivalent circuit analysis to Nyquist plots using the Z-view software: R_s[R_{bulk}/C_{bulk} [R_{CT}/C_{ss}]] (**Figure 3d**). Regarding the equivalent circuit, it is important to point out that some approximations was applied to adequately fit the measured data. As the system is composed by non-ideal capacitors, it was necessary to introduce

a CPE (constant phase element) in the equivalent circuit for fit optimization, with exponential factors ≥ 0.8 . This case, from the general CPE equation $(Z_{CPE} = [Y_0(j\omega)^n]^{-1}$, it is well-know that the exponential factor n ~ 1 describes an ideal capacitor, thus the fit simulation can be easily approximated to a simple capacitor.

The H-4h photoanodes showed reduced charge transfer resistance at the solid-liquid interface. On the other hand, the increase in R_{CT} for SH-2h suggests the creation of trapping states at the surface that suppresses the OER. Moreover, SH-4h shows a favorable surface for the OER because of its lower charge transfer resistance, revealing a possible determinant process: passivating trapping states mediated by the SH-approach or including few surface states that improve the kinetics. In this sense, the determining factors of the photoassisted processes on the designed hematite photoanode surfaces with different thicknesses were investigated in detail.

Photoresponse (J_{photo}) is a function determined by the current provided by the absorption efficiency (J_{abs}) and the global efficiency (η_{global}), which is defined by intrinsic and coupled processes, as shown in Equation 1.³⁹

$$J_{photo} = J_{abs}$$
. η_{global} , and $J_{abs} = -q\emptyset(1 - exp^{-\int \alpha l \, d\lambda})$, (1)

where α is the absorption coefficient, l is the thickness, q is the elementary charge and \emptyset is the photon flux provide at AM 1.5G. The absorbance curves from 320-720 nm were presented in the **Figure S2** (**Supporting Information**) and the absorption efficiencies (J_{abs}) of H-2h, H-4h, SH-2h and SH-4h were estimated to be 3.22, 5.52, 3.15 and 5.47 mA cm⁻², respectively. In this sense, **Figure 4** shows the global efficiency of the hematite photoanodes estimated from the photocurrent normalized by J_{abs} , revealing insights in the real performance. Despite the difference in J_{abs} , η_{global} ensures that the sonication process affects the surface efficiency provided by surface hydroxylation. This observation implies that the charge transport process may have been slightly

different from the water oxidation reaction occurring at the solid-liquid interface in these hematite samples.

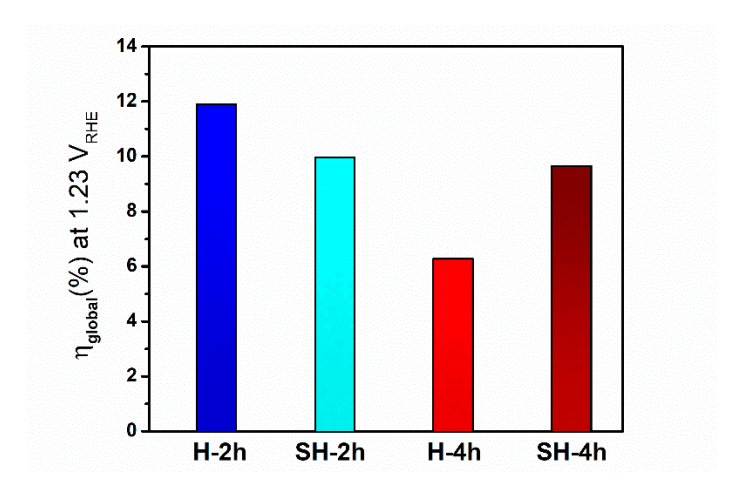


Figure 4. Calculated global efficiency (η_{global}) at 1.23 V_{RHE} applied potential for the hematite photoanodes.

The ratio between the photocurrents obtained in the absence and presence of H_2O_2 provides important information on the charge injection efficiency ($\eta_{inj} = J_{ph}/J_{H2O2}$) of each photoanode. **Figure S3 (bottom panel, Supporting Information)** clearly shows that there is no obvious difference in n_{inj} between H-2h and SH-2h. On the other hand, SH-4h showed increased injection efficiency compared to H-4h over the entire applied potential range. The injection efficiency is directly associated with the quality of the surface for hole collection mediated by favorable surface states; as a result, SH-4h has a better catalytic performance.

Furthermore, as observed in **Figure S3** (**top panel, Supporting Information**), the hematite samples responded differently in terms of charge separation efficiency ($\eta_{sep} = J_{H2O2}/J_{obs}$) before and after the surface hydroxylation process. It was noticed that the η_{sep} of H-2h decreased after sonication, which suggests that, for thinner photoanodes, the UST effect is more sensitive to the structure, revealing electron trapping states that hinder electron transport to the back contact. H-4h, for instance, increased η_{sep} after the UST process, confirming a reduced energetic barrier for

charge transport in thicker samples. η_{sep} involves kinetic parameters intrinsic to the semiconductor, in which its increase is directly associated with an increase in the lifetime and mobility of the photogenerated carriers, where the pronounced increment in η_{sep} is mainly associated with doping or a reduction in the energy barrier at homo-interfaces along with the bulk structure. The comparative analysis between the photocurrent response before and after surface hydroxylation and the global efficiency suggests that the improved PEC performance of SH-4h is the majority due to the increase in the injection efficiency.

At this point, it was clarified that the differences observed in the photoelectrochemical properties due to the thickness variation are unquestionable, where the hydroxylated surface plays a determinant role in the final performance. Thus, to probe the surface chemistry of nanowire and its coordination structures before and after ultrasonic treatment, XPS studies were performed. Fe 2p spectrum showed the orbital splitting with a $Fe2p_{3/2}$ and $Fe2p_{1/2}$ peaks centered at 710.67 ± 0.06 eV and 724.3 ± 0.03 eV, respectively, with no obvious difference between hematite photoanodes (**Figure 5a**). The results revealed a majority presence of Fe^{3+} confirmed by the well-defined satellite peak for Fe2p 3/2 orbital displaced ~8.5 eV from the hematite main peak.

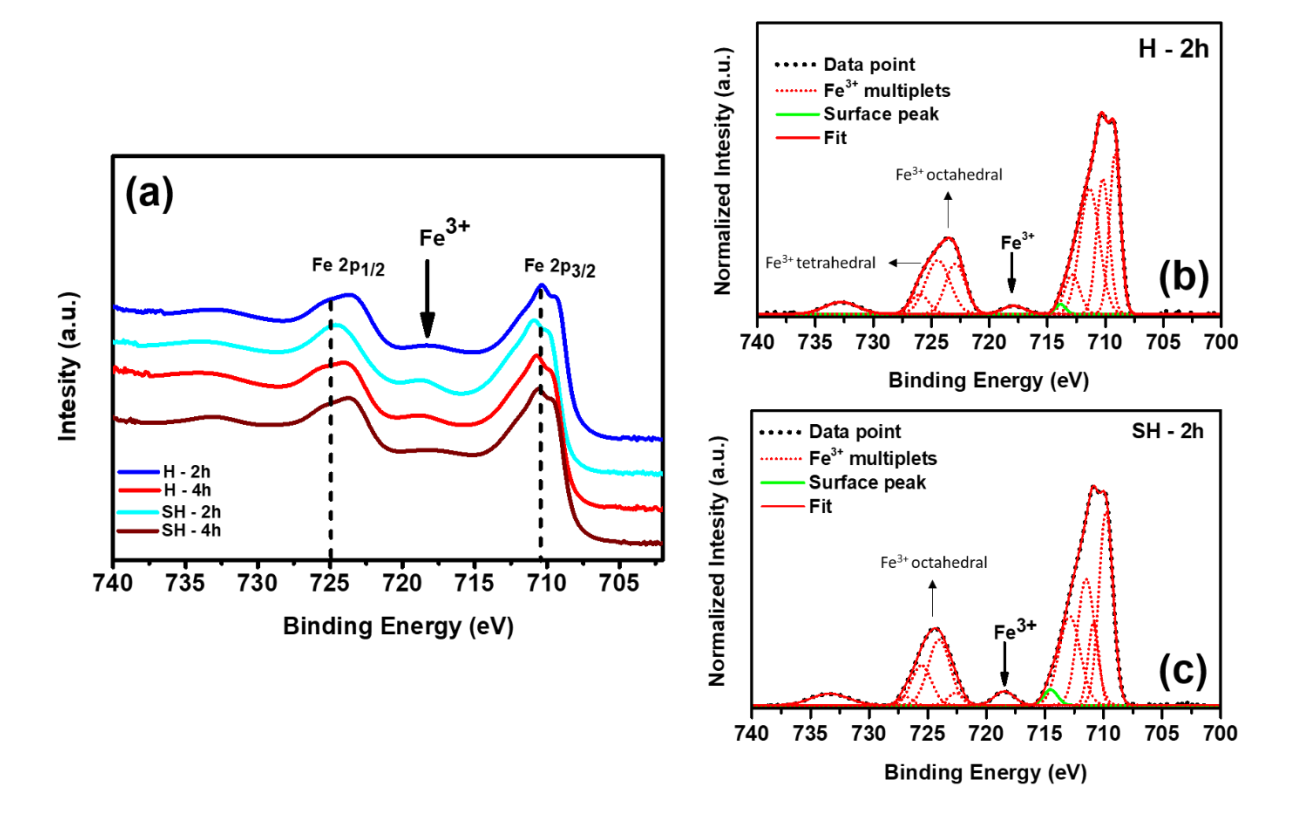


Figure 5. (a) Fe 2p core-level X-ray photoelectron spectra of hematite samples. The black arrow highlights the signal of Fe³⁺ species; (b) H-2h and (c) SH-2h spectra with deconvoluted peaks and observed Fe³⁺ ions coordination.

A detailed investigation of the Fe 2p spectrum is shown in **Figures 5b-c** and **Figure S4** (**Supporting Information**). By comparing the hematite samples before and after UST, some peculiarities can be noticed and can become decisive in the final application. SH-2h compared to H-2h, in particular, there was an increase in the surface peak (green curve) by ~50%, which is different from that observed between H-4h and SH-4h (**Figure S4, Supporting Information**). As previously discussed in the literature, the presence of a surface peak is associated with the Fe³⁺ ion neighborhood surrounded by a lower electron density, requiring greater energy to produce a photoelectron.⁴¹

Clearly, the asymmetric characteristic of the Fe $2p_{1/2}$ peak was altered for SH-2h, revealing a decrease in the iron coordination induced by UST. It is known that in the α-Fe₂O₃ structure, the ions are octahedrally and the apparent tetrahedral portion can be clarified by the presence of surface defects. 41-43 As shown in Figure 5, H-2h exhibits an asymmetry with a pronounced displacement at higher energies, which indicates a significant contribution of tetrahedral Fe³⁺, although octahedral Fe³⁺ contribution remains predominant. In contrast, SH-2h showed a greater contribution of Fe³⁺ octahedra, suggesting the removal of defective states, probably filled by OH. This trend was not followed by SH-4h and the results are shown in the supplementary data (Figure **S4, Supporting Information**). In fact, the hematite efficiency for photo-applications is associated with a defective surface, where the surface states have an important role in the oxygen evolution reactions working as mediated sites.⁶ Furthermore, the interaction strength with water molecules in iron oxide is strictly dependent on the coordination of Fe³⁺ and the coexistence of oxygen and iron ions in the upper layer.³² These results suggested that the similarities presented by the assynthesized H-2h and H-4h were not maintained after the UST process. Similar surfaces could exhibit the dynamics of energetically distinct surface states after ultrasonic treatment.

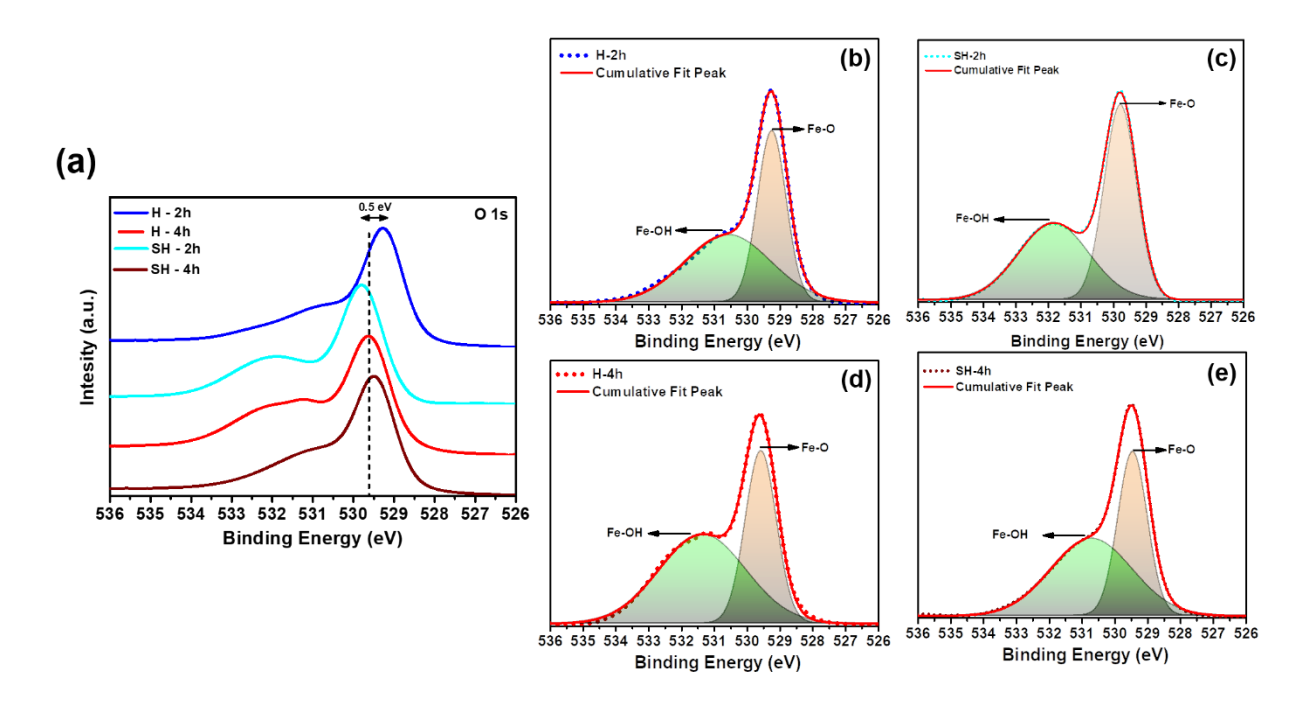


Figure 6. (a) O1s XPS profile of hematite samples. (b-e) Corresponding deconvoluted O 1s XPS profiles.

We further investigated the O1s profiles of hematite samples before and after the UST process. As shown in **Figure 6**, the core-level O1s spectra revealed a centered peak at 529-530 eV attributed to the signal of oxygen in the Fe₂O₃ crystal lattice (Fe-O bonds). In addition, the observed shoulder at higher binding energy was ascribed to the adsorbed OH species. In fact, all samples exhibited similar spectra with well-defined lattice oxygen and surface hydroxyl profiles. Specifically, H-2h presented a lower oxygen lattice binding energy with a displacement of ~0.5 eV. This indicates that H-2h has a more stoichiometric surface with a lower concentration of vacancies. Moreover, this shift towards lower energy can be associated with an upward band bending related to the Fermi level closer to the conduction band minimum. 46

Figure 6b-e present the deconvoluted O1s spectra, in order to detail the profile before and after modification. In general, the surface of hematite samples has answered differently to hydroxylation, where: (i) SH-2h revealed maintenance of the proportion of the hydroxyl signal compared with H-2h, and (ii) SH-4h decreased the ratio of Fe-OH state resulting in a smoothed

shoulder. To confirm this evidence, we collected XPS spectra from three different regions over hematite samples. We noticed an inhomogeneous contribution of Fe-OH bonds (**Figure S5**, **Supporting Information**). Interestingly, the SH-4h surface altered the hydroxyl signal depending on the region, reinforcing the inhomogeneity of hydroxylation. This trend was not observed for SH-2h, where the surface showed similar to H-2h. These results indicate that the modification is dependent on the manufacturing process time, which can be associated with the concentration of unfilled states on the precursor sample.

As previously reported, it was observed that even for a long sonication time, the surface symmetry was maintained, as evidenced in the valence band spectrum (**Figure S6a, Supporting Information**). In this sense, in the valence band profile, the first sharp peak at lower binding energy indicates that the crystal field was equally distributed around the iron atoms, which confirms the crystallization into the hematite phase.⁴⁷ While the O1s profile (**Figure S6b-c, Supporting Information**) presents a lower peak definition composed of adsorbed water, Fe-OH and Fe-O. XPS analysis showed that the impact of the mechanical process induced by sonication on the hematite nanowire surface does not contribute to the loss of surface symmetry (even for an extended sonication process), confirming that the only clear effect on the solid-liquid interface is related to the incorporation of OH states.

To investigate the impact of UST treatment on the charge carrier dynamics of these hematite photoanodes, transient absorption spectroscopy (TAS) measurements were performed (**Figure 7** and **Figure S7**). The measurement was carried out under no bias condition, see Figure S7 a-b. In open circuit condition, it was not observed evident changes in the photogenerated charge lifetime, either for thin or thick photoanodes, with only small deviations in intensity.

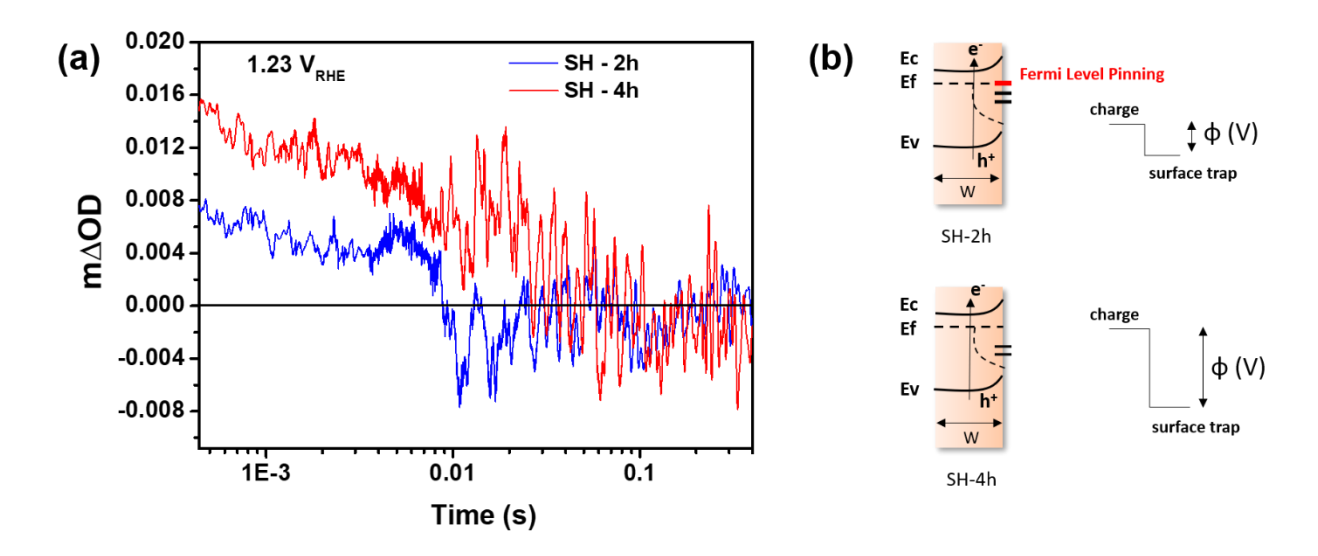


Figure 7. (a) Hole lifetime analysis by TAS using a pump of 337 nm and probe 650 nm in alkaline medium (1M NaOH) at an applied potential of 1.23 V_{RHE} for SH-2h (blue) and for SH-4h (red); (b) Schematic energy diagram for SH-2h and SH-4h.

Further analysis was performed under 1.23 V_{RHE} applied potential showing the TA spectra for surface hydroxylated photoanodes (**Figure 7a**). It was noticed that the SH-2h have presented a strong decay after 10 ms (already observed in literature)⁴⁸, which reveals a lower carrier lifetime compared to SH-4h. The enhancement in charge carrier lifetime observed for thicker materials consequently provides more time for the charge to be collected and promote the chemical reaction at the oxide photoanode surface. Thus, the best photoelectrochemical performance measured for the SH-4h can be essentially attributed to the enhanced charge carrier lifetime.

As the present idea of the charge dynamics for the synthesized photoanodes, **Figure 7b** shows a schematic band diagram where the ultrasonic treatment contribution is summarized. After the UTS, a Fermi level pinning due to the saturation of surface states for H-2h is noticeable, which explains the observed discrepancy in the LSV curves and TAS decay under applied potential, representing a competitive transport for photogenerated pairs. On the other hand, for the thicker

photoanodes (H-4h), the inclusion of the surface states after ultrasonic treatment contributes to the overall energetic distribution at the solid-liquid interface, increasing the presence of catalytic states, which results in faster OER kinetics(observed in the photo/electrochemical measurements and TAS).

In this work, it was clearly observed that thin photoanodes are quite sensitive to the manufacturing and subsequent ultrasound processes. The stress acquired between TCO/oxide layer under ultrasound directly reflects their efficiency in charge transport due to the possible complete detachment of the oxide layer from the substrate.⁴⁹ As a consequence, no charge is transported from bulk to back contact, losing an effective charge transport (or charge carrier mobility). This effect seems to be less pronounced in thicker photoanodes, while the surface effect becomes dominant. The important message here is associated with the surface hydroxylation process at thinner photoanodes, which may not lead to a positive property accumulation when subjected to mechanical stress processes. However, considering the absorption of the solar spectrum in its entirety, device applications constituting thick layers are more attractive for sufficient absorption. In this scenario, although the hydroxylation process is not extended for thinner (or ultra-thin) materials, it remains a great strategy for thicker materials, making them more active. However, for fundamental studies that require thin materials, the gain is not the same. Finally, we return to the presented duality on the role of OH states at the hematite surface, and we conclude that it will be dependent on the photoelectrode design.

4. Conclusions

This work has clearly demonstrated how different photoanode thicknesses are affected by surface modification mediated by ultrasonic treatment, creating an inhomogeneous distribution of defects based on the solid-liquid energetics. The thicker photoanodes (H-4h) showed that the mechanical

process can contribute to the removal of unstable layers, creating favorable sites for oxygen evolution without compromising the solid-solid interface. On the other hand, the ultrasonic approach for H-2h promoted surface state pinning and possibly increased the stress between hematite-FTO. The effects on thinner photoanodes (H-2h) can drastically create polarized states that enhance the surface trapping states and reduce the photogenerated charge lifetime. The gain of surface hydroxylation versus the inhomogeneity of hematite surface is mandatory to this ultrasonic approach not being possible to extend positive contributions for all hematite photoanodes differently designed. However, the technique is very satisfactory for thicker photoanodes, proving that the initial surface energy distribution, before ultrasonic treatment, is a determinant on the final PEC performance.

5. Acknowledgements

The authors acknowledge the financial support from the Brazilian agencies FAPESP (proc. 2017/25935-3 and 2014/11736-0), CAPES, CEM-UFABC, and CDMF (grant 2013/072962). We are thankful for all support form UCSC (Santa Cruz – USA) during this collaboration, specially to the Chemistry & Biochemistry department. A.L.M.F and F.L.S gratefully acknowledge support from FAPESP (Grant 2017/11986-5) and Shell and the strategic importance of the support given by ANP (Brazil's National Oil, Natural Gas and Biofuels Agency) through the R&D levy regulation. Y.L. thanks the financial support from the National Science Foundation under grant no. DMR-2003563. We also acknowledge Saulo A. Carminati and Dr. Ana F. Nogueira for the TAS spectroscopy at IQ-Unicamp.

6. References

(1) Vayssieres, L.; Keis, K.; Lindquist, S.-E.; Hagfeldt, A. Purpose-Built Anisotropic Metal Oxide Material: 3D Highly Oriented Microrod Array of ZnO. *J. Phys. Chem. B* **2001**, *105*

- (17), 3350–3352.
- (2) Bassi, P. S.; Gurudayal; Wong, L. H.; Barber, J. Iron Based Photoanodes for Solar Fuel Production. *Phys. Chem. Chem. Phys.* **2014**, *16* (24), 11834.
- (3) Shen, S.; Lindley, S. A.; Chen, X.; Zhang, J. Z. Hematite Heterostructures for Photoelectrochemical Water Splitting: Rational Materials Design and Charge Carrier Dynamics. *Energy Environ. Sci.* **2016**, *9* (9), 2744–2775.
- (4) Sivula, K.; Le Formal, F.; Grätzel, M. Solar Water Splitting: Progress Using Hematite (α-Fe(2) O(3)) Photoelectrodes. *ChemSusChem* **2011**, *4* (4), 432–449.
- (5) Souza, F. L.; Leite, E. R. Latest Advances on the Columnar Nanostructure for Solar Water Splitting. In *Nanoenergy*; Springer International Publishing: Cham, 2018; Vol. 55, pp 141–160.
- (6) Iandolo, B.; Hellman, A. The Role of Surface States in the Oxygen Evolution Reaction on Hematite. *Angew. Chemie Int. Ed.* **2014**, *53* (49), 13404–13408.
- (7) Zhang, J.; Eslava, S. Understanding Charge Transfer, Defects and Surface States at Hematite Photoanodes. *Sustain. Energy Fuels* **2019**, *3* (6), 1351–1364.
- (8) Appavoo, K.; Liu, M.; Black, C. T.; Sfeir, M. Y. Quantifying Bulk and Surface Recombination Processes in Nanostructured Water Splitting Photocatalysts via in Situ Ultrafast Spectroscopy. *Nano Lett.* **2015**, *15* (2), 1076–1082.
- (9) Gong, L.; Xie, J.; Liang, X.; Xiong, J.; Yi, S.; Zhang, X.; Li, C. M. Tailoring Surface States by Sequential Doping of Ti and Mg for Kinetically Enhanced Hematite Photoanode. *J. Colloid Interface Sci.* **2019**.
- (10) Lopes, T.; Andrade, L.; Le Formal, F.; Gratzel, M.; Sivula, K.; Mendes, A. Hematite Photoelectrodes for Water Splitting: Evaluation of the Role of Film Thickness by

- Impedance Spectroscopy. Phys. Chem. Chem. Phys. 2014, 16 (31), 16515.
- (11) Freitas, A. L. M.; Carvalho, W. M.; Souza, F. L. Enhanced Water Oxidation Efficiency of Hematite Thin Films by Oxygen-Deficient Atmosphere. *J. Mater. Res.* **2015**, *30* (23), 3595–3604.
- (12) Forster, M.; Potter, R. J.; Ling, Y.; Yang, Y.; Klug, D. R.; Li, Y.; Cowan, A. J. Oxygen Deficient α-Fe 2 O 3 Photoelectrodes: A Balance between Enhanced Electrical Properties and Trap-Mediated Losses. *Chem. Sci.* 2015, 6 (7), 4009–4016.
- (13) Ling, Y.; Wang, G.; Reddy, J.; Wang, C.; Zhang, J. Z.; Li, Y. The Influence of Oxygen Content on the Thermal Activation of Hematite Nanowires. *Angew. Chemie Int. Ed.* **2012**, 51 (17), 4074–4079.
- (14) Ling, Y. C.; Wang, G. M.; Wheeler, D. A.; Zhang, J. Z.; Li, Y. Hematite Nanostructures for Photoelectrochemical Water Splitting. *Abstr. Pap. Am. Chem. Soc.* **2011**, *242*, 2119–2125.
- (15) Carvalho, W. M.; Souza, F. L. Hematite Surface Activation by Chemical Addition of Tin Oxide Layer. *ChemPhysChem* **2016**, 2710–2717.
- (16) Jeon, T. H.; Bokare, A. D.; Han, D. S.; Abdel-Wahab, A.; Park, H.; Choi, W. Dual Modification of Hematite Photoanode by Sn-Doping and Nb2O5 Layer for Water Oxidation. *Appl. Catal. B Environ.* 2017, 201, 591–599.
- (17) Kronawitter, C. X.; Zegkinoglou, I.; Shen, S. H.; Liao, P.; Cho, I. S.; Zandi, O.; Liu, Y. S.; Lashgari, K.; Westin, G.; Guo, J. H.; et al. Titanium Incorporation into Hematite Photoelectrodes: Theoretical Considerations and Experimental Observations. *Energy and Environmental Science*. 2014, 7, 3100-3121.
- (18) Tofanello, A.; Diao, Z.; Djatoubai, E.; Su, J. Z.; Shen, S. H.; Souza, F. L.; Vayssieres, L. Engineering Hematite/Plasmonic Nanoparticle Interfaces for Efficient

- Photoelectrochemical Water Splitting. J. Appl. Phys. 2020, 128 (6), 063103.
- (19) Sivula, K.; Zboril, R.; Le Formal, F.; Robert, R.; Weidenkaff, A.; Tucek, J.; Frydrych, J.; Grätzel, M. Photoelectrochemical Water Splitting with Mesoporous Hematite Prepared by a Solution-Based Colloidal Approach. *J. Am. Chem. Soc.* **2010**, *132* (21), 7436–7444.
- (20) Souza, F. L.; Xavier, A. M.; De Carvalho, W. M.; Gonçalves, R. H.; Leite, E. R. Facile Routes to Produce Hematite Film for Hydrogen Generation from Photoelectro-Chemical Water Splitting. In *Nanoenergy: Nanotechnology Applied for Energy Production*; 2013, 81-99.
- (21) Gonçalves, R. H.; Leite, E. R. Nanostructural Characterization of Mesoporous Hematite Thin Film Photoanode Used for Water Splitting. *J. Mater. Res.* **2014**, *29* (1), 47–54.
- (22) Li, M.; Yang, Y.; Ling, Y.; Qiu, W.; Wang, F.; Liu, T.; Song, Y.; Liu, X.; Fang, P.; Tong, Y.; et al. Morphology and Doping Engineering of Sn-Doped Hematite Nanowire Photoanodes. *Nano Lett.* **2017**, *17* (4), 2490–2495.
- (23) Ling, Y.; Wang, G.; Wheeler, D. A.; Zhang, J. Z.; Li, Y. Sn-Doped Hematite Nanostructures for Photoelectrochemical Water Splitting. *Nano Lett.* **2011**, *11* (5), 2119–2125.
- (24) Nogueira, A. E.; Soares, M. R. S.; Souza Junior, J. B.; Ospina, C.; Souza, F. L.; Leite, E. R. Discovering a Selective Semimetal Element to Increase Hematite Photoanode Charge Separation Efficiency. *J. Mater. Chem. A* 2019, 7 (28), 16992–16998.
- (25) Bedin, K. C.; Freitas, A. L. M.; Tofanello, A.; Rodríguez-Gutiérrez, I.; Souza, F. L. Revealing the Synergy of Sn Insertion in Hematite for Next-generation Solar Water Splitting Nanoceramics. *Int. J. Ceram. Eng. Sci.* **2020**, *2* (5), 204–227.
- (26) Li, M.; Liu, T.; Yang, Y.; Qiu, W.; Liang, C.; Tong, Y.; Li, Y. Zipping Up NiFe(OH) *x* Encapsulated Hematite To Achieve an Ultralow Turn-On Potential for Water Oxidation.

- ACS Energy Lett. 2019, 4 (8), 1983–1990.
- (27) Freitas, A. L. M.; Muche, D. N. F.; Leite, E. R.; Souza, F. L. Interface Engineering of Nanoceramic Hematite Photoelectrode for Solar Energy Conversion. *J. Am. Ceram. Soc.* 2020, 103 (12), 6833–6846.
- (28) JagannathanMadhavan; JayaramanTheerthagiri; DhandapaniBalaji; SallaSunitha; Choi; MuthupandianAshokkumar. Hybrid Advanced Oxidation Processes Involving Ultrasound: An Overview. *Molecules* **2019**, *24* (18), 3341.
- (29) Riesz, P.; Berdahl, D.; Christman, C. L. Free Radical Generation by Ultrasound in Aqueous and Nonaqueous Solutions. *Environ. Health Perspect.* **1985**, *64*, 233–252.
- (30) Tang, C.; Sun, B.; Li, M.; Zhang, J.; Fan, X.; Gao, F.; Tong, Y.; Dong, L.; Li, Y. Surface Hydroxylated Hematite Promotes Photoinduced Hole Transfer for Water Oxidation. *J. Mater. Chem. A* **2019**, *7* (14), 8050–8054.
- (31) Rehman, M. U.; Jawaid, P.; Uchiyama, H.; Kondo, T. Comparison of Free Radicals Formation Induced by Cold Atmospheric Plasma, Ultrasound, and Ionizing Radiation. *Arch. Biochem. Biophys.* **2016**, *605*, 19–25.
- (32) Ovcharenko, R.; Voloshina, E.; Sauer, J. Water Adsorption and O-Defect Formation on Fe2O3(0001) Surfaces. *Phys. Chem. Chem. Phys.* **2016**, 18, 25560-25568.
- (33) Jain, S.; Shah, J.; Negi, N. S.; Sharma, C.; Kotnala, R. K. Significance of Interface Barrier at Electrode of Hematite Hydroelectric Cell for Generating Ecopower by Water Splitting. *Int. J. Energy Res.* **2019**, *43* (9), 4743–4755.
- (34) de Carvalho, V. A. N.; Luz, R. A. de S.; Lima, B. H.; Crespilho, F. N.; Leite, E. R.; Souza, F. L. Highly Oriented Hematite Nanorods Arrays for Photoelectrochemical Water Splitting.
 J. Power Sources 2012, 205, 525–529.

- (35) Li, Y.; Chen, H. Facile Fire Treatment of Nanostructured Hematite with an Enhanced Photoelectrochemical Water Splitting Performance. *J. Mater. Chem. A* **2016**, *4* (39), 14974–14977.
- (36) Fàbrega, C.; Monllor-Satoca, D.; Ampudia, S.; Parra, A.; Andreu, T.; Morante, J. R. Tuning the Fermi Level and the Kinetics of Surface States of TiO 2 Nanorods by Means of Ammonia Treatments. *J. Phys. Chem. C* **2013**, *117* (40), 20517–20524.
- Muche, D. N. F.; dos Santos, T. M. G.; Leite, G. P.; Melo, M. A.; Gonçalves, R. V.; Souza,
 F. L. Tailoring Hematite/FTO Interfaces: New Horizons for Spin-Coated Hematite
 Photoanodes Targeting Water Splitting. *Mater. Lett.* 2019, 254, 218–221.
- (38) Klahr, B.; Gimenez, S.; Fabregat-Santiago, F.; Hamann, T.; Bisquert, J. Water Oxidation at Hematite Photoelectrodes: The Role of Surface States. *J. Am. Chem. Soc.* **2012**, *134* (9), 4294–4302.
- (39) Zandi, O.; Hamann, T. W. The Potential versus Current State of Water Splitting with Hematite. *Phys. Chem. Chem. Phys.* **2015**, *17* (35), 22485–22503.
- Ito, N. M.; Carvalho, W. M.; Muche, D. N. F.; Castro, R. H. R.; Dalpian, G. M.; Souza, F.
 L. High Temperature Activation of Hematite Nanorods for Sunlight Driven Water
 Oxidation Reaction. *Phys. Chem. Chem. Phys.* 2017, 19 (36), 25025–25032.
- (41) Grosvenor, A. P.; Kobe, B. A.; Biesinger, M. C.; McIntyre, N. S. Investigation of Multiplet Splitting of Fe 2p XPS Spectra and Bonding in Iron Compounds. *Surf. Interface Anal.* **2004**, 36, 1564-1574.
- (42) Droubay, T.; Chambers, S. A. Surface-Sensitive Fe2p Photoemission Spectra for α- Fe2O3
 (0001): The Influence of Symmetry and Crystal-Field Strength. *Phys. Rev. B* 2001, 64 (20), 205414.

- (43) Chernyshova, I. V.; Hochella, M. F.; Madden, A. S. Size-Dependent Structural Transformations of Hematite Nanoparticles. 1. Phase Transition. *Phys. Chem. Chem. Phys.* **2007**, 9, 1736-1750.
- (44) Wu, H.; Yang, T.; Du, Y.; Shen, L.; Ho, G. W. Identification of Facet-Governing Reactivity in Hematite for Oxygen Evolution. *Adv. Mater.* **2018**, *30* (52), 1804341.
- (45) Tao, H. B.; Fang, L.; Chen, J.; Yang, H. Bin; Gao, J.; Miao, J.; Chen, S.; Liu, B. Identification of Surface Reactivity Descriptor for Transition Metal Oxides in Oxygen Evolution Reaction. J. Am. Chem. Soc. 2016, 38(31) 9978–9985.
- (46) Kraushofer, F.; Jakub, Z.; Bichler, M.; Hulva, J.; Drmota, P.; Weinold, M.; Schmid, M.; Setvin, M.; Diebold, U.; Blaha, P.; et al. Atomic-Scale Structure of the Hematite α-Fe2O3(11-02) "r-Cut" Surface. J. Phys. Chem. C 2018, 122(3) 1657–1669.
- (47) Lohaus, C.; Steinert, C.; Brötz, J.; Klein, A.; Jaegermann, W. Systematic Investigation of the Electronic Structure of Hematite Thin Films. *Adv. Mater. Interfaces* **2017**, *4* (20), 2–9.
- (48) Van Leeuwen, N. S.; Blom, B.; Xie, M.; Adamaki, V.; Bowen, C. R.; De Araújo, M. A.; Mascaro, L. H.; Cameron, P. J.; Marken, F. Residual Energy Harvesting from Light Transients Using Hematite as an Intrinsic Photocapacitor in a Symmetrical Cell. ACS Appl. Energy Mater. 2018, 1(1), 38–42.
- (49) Souza, F. L.; Lopes, K. P.; Nascente, P. A. P.; Leite, E. R. Nanostructured Hematite Thin Films Produced by Spin-Coating Deposition Solution: Application in Water Splitting. *Sol. Energy Mater. Sol. Cells* **2009**, 93(3), 362-368.